Journal of Alloys and Compounds 519 (2012) 15–24

Contents lists available at SciVerse ScienceDirect

Journal of Alloys and Compounds

journal homepage: www.elsevier.com/locate/jallcom

Mechanism of unique hardening of dental Ag–Pd–Au–Cu alloys in relation with constitutional phases

Yonghwan Kim[a], Mitsuo Niinomi[b,*], Masaaki Nakai[b], Toshikazu Akahori[b,1], Toru Kanno[a,2], Hisao Fukui[c]

[a] Department of Materials Science, Graduate School of Engineering, Tohoku University, 6-6 Aoba, Aramaki Aza, Aoba-ku, Sendai 980-8579, Japan
[b] Department of Biomaterials Science, Institute for Materials Research, Tohoku University, 2-1-1 Katahira, Aoba-ku, Sendai 980-8577, Japan
[c] Department of Dental Materials Science, School of Dentistry, Aichi-Gakuin University, 1-100 Kusumoto-cho, Chikusa-ku, Nagoya 464-8650, Japan

ARTICLE INFO

Article history:
Received 26 May 2011
Received in revised form 24 October 2011
Accepted 29 October 2011
Available online 22 November 2011

Keywords:
Ag–Pd–Au–Cu alloy
Liquid rapid solidification method
Unique hardening behavior
Microstructural change

ABSTRACT

The objective of this research was to investigate the effect of constitutional phases on the unique hardening behavior of as-solutionized dental Ag–Pd–Au–Cu alloy fabricated by cold rolling. The commercial dental Ag–Pd–Au–Cu alloy fabricated by cold rolling consists of Cu-rich α_1, Ag-rich α_2, and β phases. On the other hand, the Ag–Pd–Au–Cu alloy fabricated by the liquid rapid solidification (LRS) method consists of single α phase. They were subjected to various heat treatments, respectively. The microstructures were observed by scanning electron microscope, transmission electron microscope and X-ray diffraction. The hardness was evaluated by a Vickers micro-hardness tester. In the Ag–Pd–Au–Cu alloy fabricated by cold rolling, the fine $L1_0$-type-ordered β′ phase is precipitated and the coarse β phase is remained after solution treatment at 1123 K. The hardness increases drastically. On the other hand, in the Ag–Pd–Au–Cu alloy fabricated by LRS method, the single α phase was decomposed into the α_1 phase and the α_2 phase after solution treatment at 1023 K and its hardness change was small. However, after aging treatment at 673 K, the fine β phase is precipitated in the α phase and the hardness increases greatly even in the Ag–Pd–Au–Cu alloy fabricated by LRS method. It is considered that the precipitation of the fine $L1_0$-type-ordered β′ phase may contribute strongly to the unique hardening in the as-solutionized dental Ag–Pd–Au–Cu alloy fabricated by cold rolling.

1. Introduction

Ag–Pd–Au–Cu alloys have been widely used in dental applications because they are relatively cheaper and possess higher mechanical strength than gold alloys. It is well known that the Ag–Pd–Au–Cu alloy exhibits age-hardening behavior [1,2]. However, it has been reported that the hardness of Ag–20Pd–12Au–14.5Cu (mass%) alloys subjected to solution treatment (ST) at a temperature over 1073 K followed by water quenching (WQ) is drastically enhanced [3]. This unique hardening behavior has been explained as being due to two hardening mechanisms: one is the solid-solution hardening mechanism, in which alloying elements are dissolved in the matrix (α phase) by ST [3], and the other is the precipitation hardening mechanism, in which $L1_0$-type-ordered β′ phases are precipitated during the quenching process after ST [4]. However, the unique hardening mechanism is still unclear. It is difficult to investigate the contribution of the constitutional phase to the unique hardening behavior because of the multi-phase microstructure (α_1, α_2, β) of Ag–20Pd–12Au–14.5Cu alloy. Recently, it has been reported that Ag–20Pd–12Au–14.5Cu alloy can be fabricated with the α, α_1, and α_2 phases by the liquid rapid solidification (LRS) method and that the hardness of the alloy after ST changes slightly [5]. It has been reported that Ag–20Pd–14.5Cu–12Au alloys with α_1, α_2, and β phases, and Ag–20Pd–14.5Cu–12Au alloys with α, α_1, and α_2 phase show different hardening behaviors although both of them have the same chemical compositions and are subjected to the same condition of solution treatment [5]. One significant microstructural difference is the existence of a coarse Cu–Pd intermetallic compound (β phase), which is considered to contribute to the unique hardening behavior to some degree.

The microstructures and Vickers hardness of Ag–20Pd–14.5Cu–12Au alloys with single α phase fabricated by LRS subjected to various heat treatments were investigated in order to understand the effect of constitutional phases on the unique hardening behavior of as-solutionized Ag–Pd–Au–Cu alloy fabricated by cold rolling.

* Corresponding author. Tel.: +81 22 215 2574; fax: +81 22 215 2553.
E-mail address: niinomi@imr.tohoku.ac.jp (M. Niinomi).
[1] Address: Department of Materials Science and Engineering, Faculty of Science and Technology, Meijo University, 1-501 Shiogamaguchi, Tempaku-ku, Nagoya 464-0045, Japan.
[2] Address: Sharp Corp., 22-22 Nagaike-cho, Abeno-ku, Osaka 545-8522, Japan.

0925-8388/$ – see front matter © 2011 Elsevier B.V. All rights reserved.
doi:10.1016/j.jallcom.2011.10.099

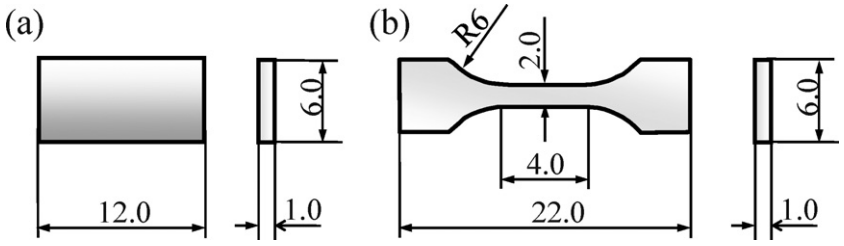

Fig. 1. Schematic drawings of specimens for (a) CR and (b) LRS in mm.

Table 1
Chemical composition of dental Ag–20Pd–12Au–14.5Cu alloy.

	Ag	Pd	Au	Cu	Others
Mass%	51.0	20.0	12.0	14.5	2.5

2. Materials and methods

2.1. Materials and heat treatment process

The materials used in this study were commercial dental Ag–20Pd–12Au–14.5Cu alloys (Ishifuku Kinpara S12, Ishifuku Metal Industry Co., Ltd, Tokyo, Japan) fabricated by cold rolling (hereafter referred to as CR) and their chemical compositions are listed in Table 1. The shape and size of Ag–20Pd–12Au–14.5Cu alloy is shown in Fig. 1(a). CR was subjected to ST at 1123 K for 3.6 ks in vacuum and then was quenched into cold water (CR-ST) as schematically shown in Fig. 2. For comparison purposes, the Ag–20Pd–12Au–14.5Cu alloy was also fabricated by LRS method (hereafter referred to as LRS) using a melting machine as schematically shown in Fig. 3 [5]. The shape and size of LRS is shown in Fig. 1(b). All LRS were subjected to ST at 1173 K for 3.6 ks in vacuum for a single α phase (1173WQ_{LRS}/3.6 ks). 1023 K is over the critical temperature for the order–disorder transformation in the Cu–Pd binary phase diagram and 1023 K is the temperature for the Cu-rich phase (α_1) and Ag-rich phase (α_2) to decompose in the Ag–Cu binary phase diagram. 1173WQ_{LRS}/3.6 ks was subjected to ST at 1023 K for t (1023WQ_{LRS}/t, t: 1.8–28.8 ks) in vacuum as schematically shown in Fig. 4. 673 K is the temperature generally used for aging treatment (AT) in Ag–Pd–Au–Cu alloys. 1173WQ_{LRS}/3.6 ks was subjected to AT at 673 K for t (673WQ_{LRS}/t, t: 1.8–28.8 ks) in vacuum as schematically shown in Fig. 5. According to the literature [3], the unique hardening behavior was observed after ST over 1073 K. 673WQ_{LRS}/1.8 ks was again subjected to ST at 1173 K for 3.6 ks in vacuum after aging treatment (AT) to confirm the existence of the unique hardening behavior in a LRS alloy with the β phase (673WQ_{LRS}/1.8 ks-ST) as schematically shown in Fig. 6.

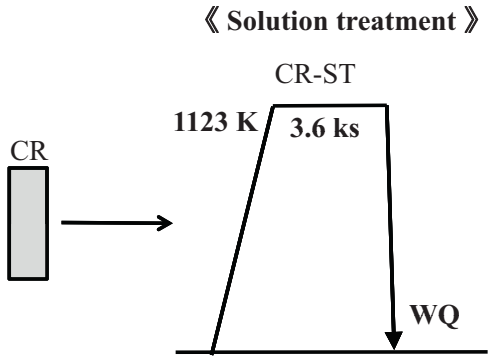

Fig. 2. Schematic drawing of solution treatment for Ag–Pd–Cu–Au alloy fabricated by cold rolling.

2.2. Microstructural observation

After all specimens were wet-polished using emery papers of up to 4000 grit, and then mirror-polished using alumina suspension, their surfaces were observed using a scanning electron microscope (SEM) with a backscattered electron (BSE) detector. The chemical compositions were investigated using an energy-dispersive X-ray spectroscopy (EDX) installed in the SEM. In addition, discs with a diameter of 3 mm and a thickness of 1 mm were cut from some specimens using wire electrical discharge machining for the transmission electron microscopic observation. These discs were ground to 50 μm thick using emery papers and alumina suspension, and were thinned by dimple grinding and ion milling. The specimens were examined using a transmission electron microscope (TEM) with an accelerating voltage of 200 kV and a high-resolution transmission electron microscope (HRTEM) with an accelerating voltage of 200 kV. X-ray diffraction (XRD) analyses of all samples were carried out using a diffractometer operating at 40 kV and 40 mA to identify the constitutional phases.

2.3. Hardness test

Hardness measurement was performed on each mirror-polished sample after SEM observation and XRD analysis using a Vickers micro-hardness tester with a

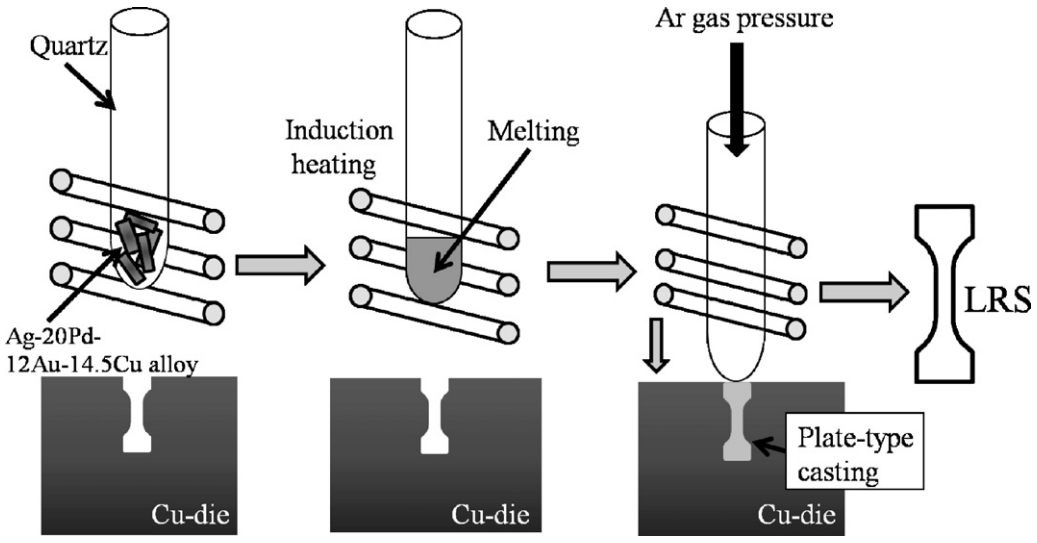

Fig. 3. Schematic drawing of liquid rapid solidification (LRS) method.

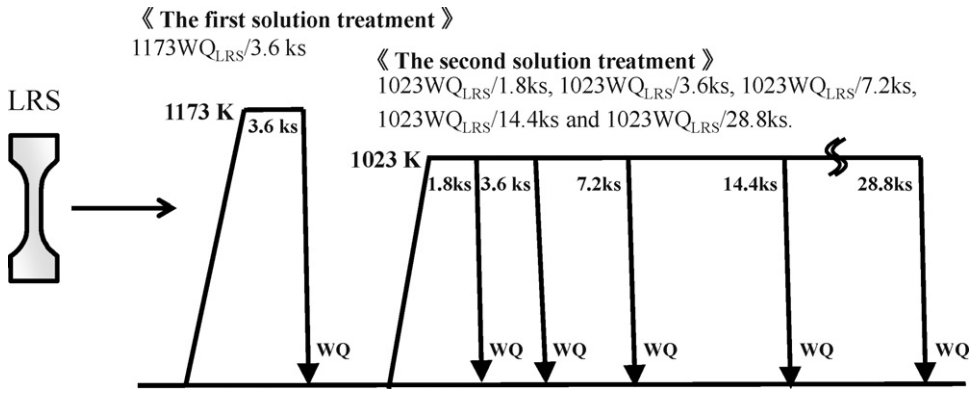

Fig. 4. Schematic drawing of solution treatment for Ag–Pd–Cu–Au alloy fabricated by LRS method.

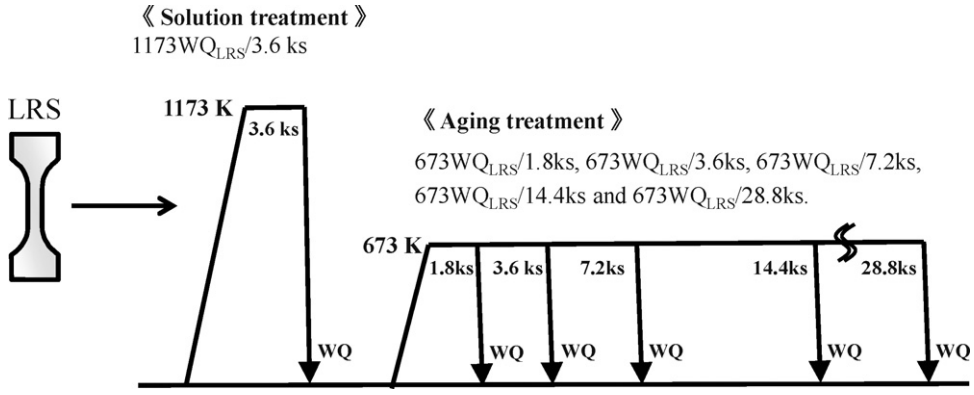

Fig. 5. Schematic drawing of aging treatment for Ag–Pd–Cu–Au alloy fabricated by LRS method.

load of 4.9 N and a holding time of 15 s. After 10 times measurements on each sample, Vickers micro-hardness (HV) was calculated to the mean value of 8 times measurements after omitting maximum and minimum values.

3. Results

3.1. Microstructure

3.1.1. Effect of solution treatment on microstructures of CR

Fig. 7 shows the XRD profiles of CR and CR-ST. α_1, α_2 and β phases are identified in CR, and α, α_2, and β phases are identified in CR-ST. Fig. 8 shows the microstructure of CR-ST by BSE image and the result of the EDX analysis. CR is composed of α_1, α_2, and β phases. After ST, the Cu-rich α_1 phase of CR was dissolved into the Ag-rich α_2 phase and the Cu–Pd intermetallic compound (β) is remained. CR-ST is composed of α, α_2, and β phases. The results of XRD analysis correspond well with the results of the BSE image and XRD analysis. Fig. 9 shows a bright field image and selected diffraction pattern of CR-ST obtained from TEM observation. The bright field image shows not only a round-shaped β phase but also a lath-shaped fine precipitate. The lath-shaped fine precipitate is confirmed to be the $L1_0$-type-ordered phase (β′) by a selected area diffraction pattern. This result agrees with those of the previous studies [4,5].

3.1.2. Effect of solution treatment on microstructures of LRS

Fig. 10 shows the XRD profiles of 1173WQ$_{LRS}$/3.6 ks and 1023WQ$_{LRS}$/1.8–28.8 ks. The single α phase is identified in 1173WQ$_{LRS}$/3.6 ks. The α, α_1, and α_2 phases are identified in 1023WQ$_{LRS}$/1.8–28.8 ks while the β phase is not identified in 1023WQ$_{LRS}$/1.8–28.8 ks.

Fig. 11 shows the microstructures of 1173WQ$_{LRS}$/3.6 ks and 1023WQ$_{LRS}$/1.8–28.8 ks by BSE images. The microstructure of 1173WQ$_{LRS}$/3.6 ks is composed of the single α phase (Fig. 11a). The

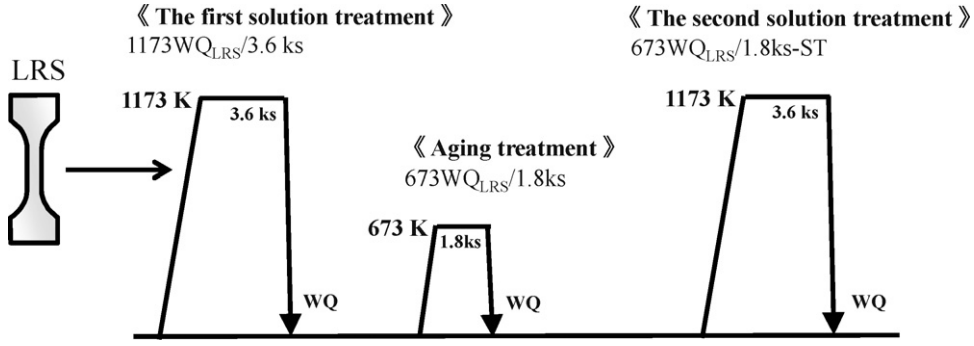

Fig. 6. Schematic drawing of solution treatment for aging-treated Ag–Pd–Cu–Au alloy by LRS method.

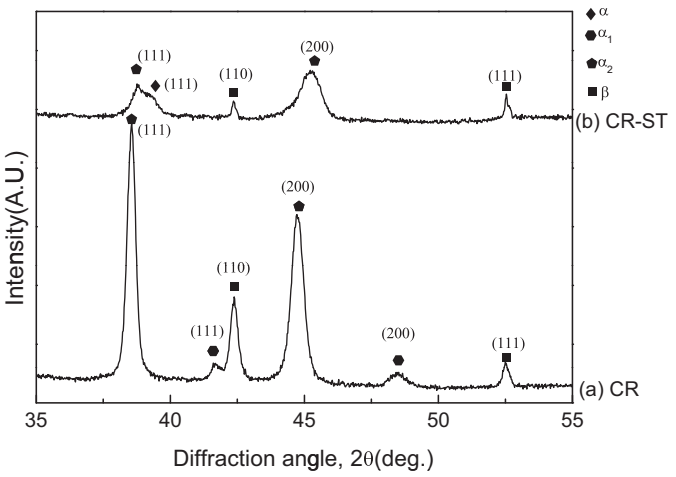

Fig. 7. XRD profiles of CR and CR-ST.

microstructures of $1023WQ_{LRS}$/1.8–28.8 ks are decomposed into two (black, white) areas corresponding to α_1 and α_2 phases from the part of single α phase with increasing time during ST at 1023 K (Fig. 11b–f). BSE image and EDX analysis shows that the microstructure of $1023WQ_{LRS}$/28.8 ks is composed of a Cu-rich α_1 phase, an Ag-rich α_2 phase, and α phase (Fig. 12). The single α phase decomposes into the Cu-rich α_1 phase and the Ag-rich α_2 phase, but the β phase is not precipitated by ST at 1023 K.

3.1.3. *Effect of aging treatment on microstructures of LRS*

Fig. 13 shows the XRD profiles of $1173WQ_{LRS}$/3.6 ks and $673WQ_{LRS}$/1.8 ks–28.8 ks. The single α phase is identified in $1173WQ_{LRS}$/3.6 ks (Fig. 13a). The α, α_1, and α_2 phases are changed to α_2 and β phases during AT at 673 K (Fig. 13b–f).

Fig. 14 shows the microstructures of $1173WQ_{LRS}$/3.6 ks and $673WQ_{LRS}$/1.8–28.8 ks obtained by BSE images. The microstructure of $1173WQ_{LRS}$/3.6 ks is a single α phase. The weak contrast in the BSE images of $673WQ_{LRS}$/1.8–14.4 ks (Fig. 14(b–e)) appears after aging treatment. This is considered to the result from the chemical composition difference; the area where the β phase precipitates

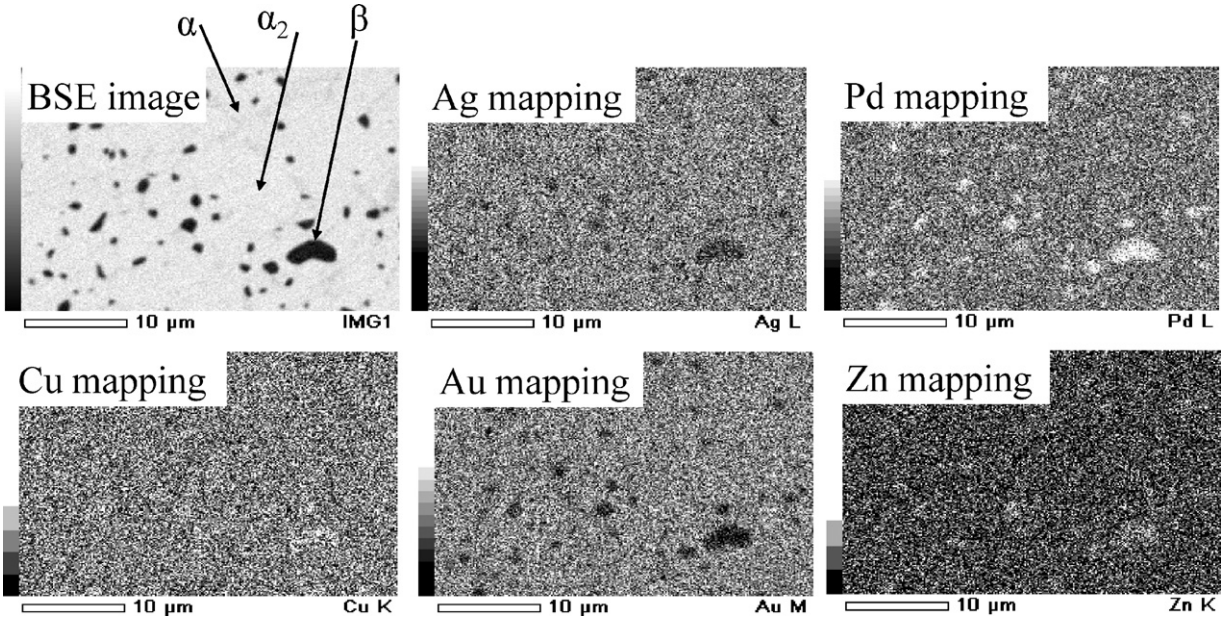

Fig. 8. BSE image and results of EDX analysis on specimen surface of CR-ST.

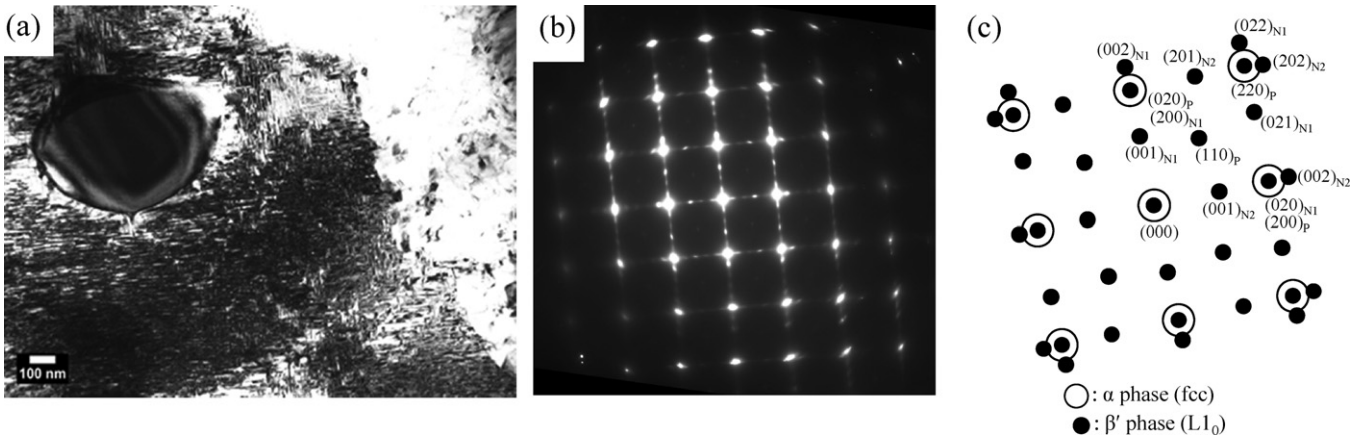

Fig. 9. Results of TEM observation of CR-ST: (a) bright field image, (b) selected area diffraction pattern and (c) key diagram. Beam direction is parallel to [1 0 0]. In this key diagram, three variants of the $L1_0$-type-ordered phase are superimposed: one with the *c*-axis parallel to the electron beam (P), and two with their *c*-axes normal to the electron beam (N_1, N_2) [1].

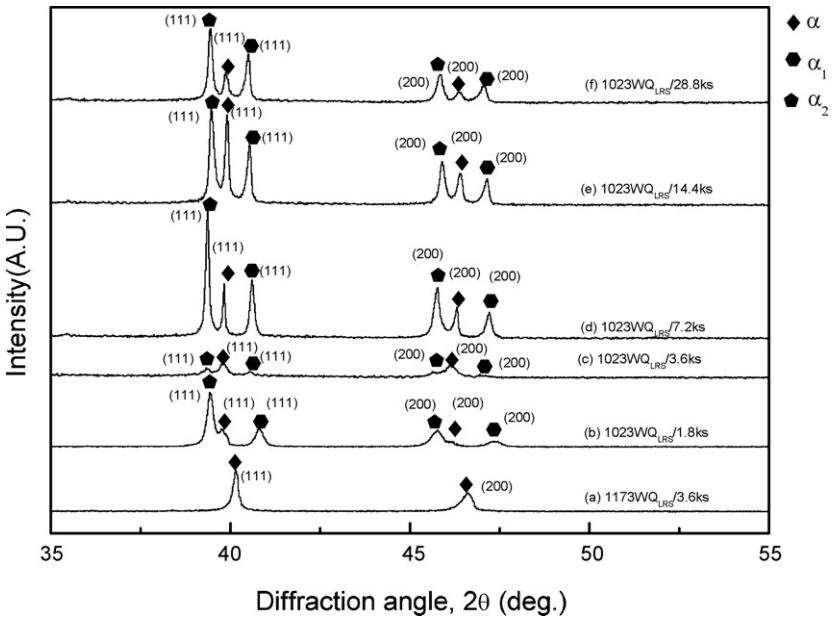

Fig. 10. XRD profiles of (a) 1173WQ_{LRS}/3.6 ks, (b) 1023WQ_{LRS}/1.8 ks, (c) 1023WQ_{LRS}/3.6 ks, (d) 1023WQ_{LRS}/7.2 ks, (e) 1023WQ_{LRS}/14.4 ks and (f) 1023WQ_{LRS}/28.8 ks.

and the area where the β phase does not precipitate exist after aging treatment.

Fig. 15 shows a bright field image, a dark field image, a selected area diffraction, and a key diagram of 673WQ_{LRS}/1.8 ks. The selected area diffraction pattern shows the existence of the α phase and the β phase. The dark field image is obtained using a (0 1 0) superlattice reflection from the B2-type ordered β phase. The β phase less than 100 nm long is precipitated in the matrix.

XRD profiles show that the peaks of α, α_2 and β phases of 673WQ_{LRS}/1.8 ks with the β phase subjected to ST at 1173 K for 3.6 ks are changed to the peak of the single α phase (Fig. 16) and the contrast in BSE image of 673WQ_{LRS}/1.8 ks is disappeared (Fig. 17) by ST at 1173 K for 3.6 ks. These imply that the

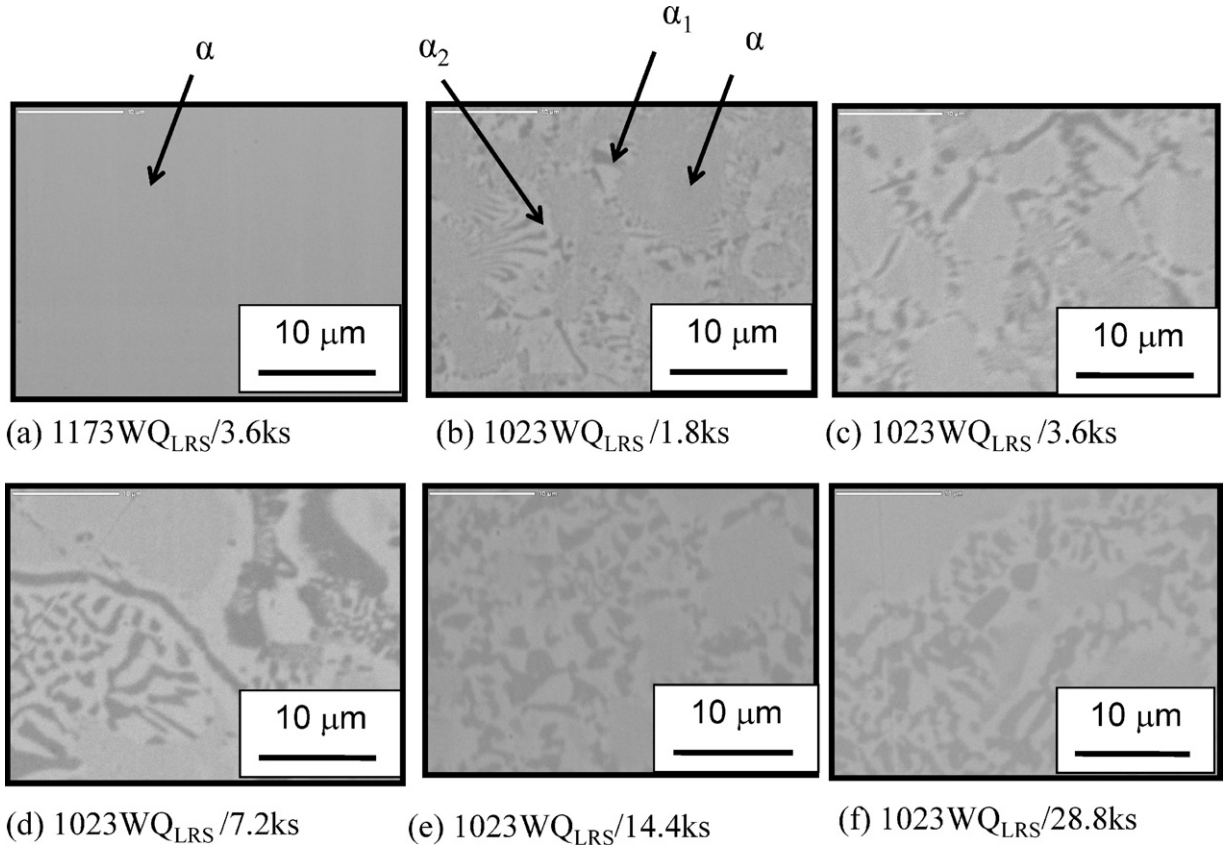

Fig. 11. BSE images of (a) 1173WQ_{LRS}/3.6 ks, (b) 1023WQ_{LRS}/1.8 ks, (c) 1023WQ_{LRS}/3.6 ks, (d) 1023WQ_{LRS}/7.2 ks, (e) 1023WQ_{LRS}/14.4 ks and (f) 1023WQ_{LRS}/28.8 ks.

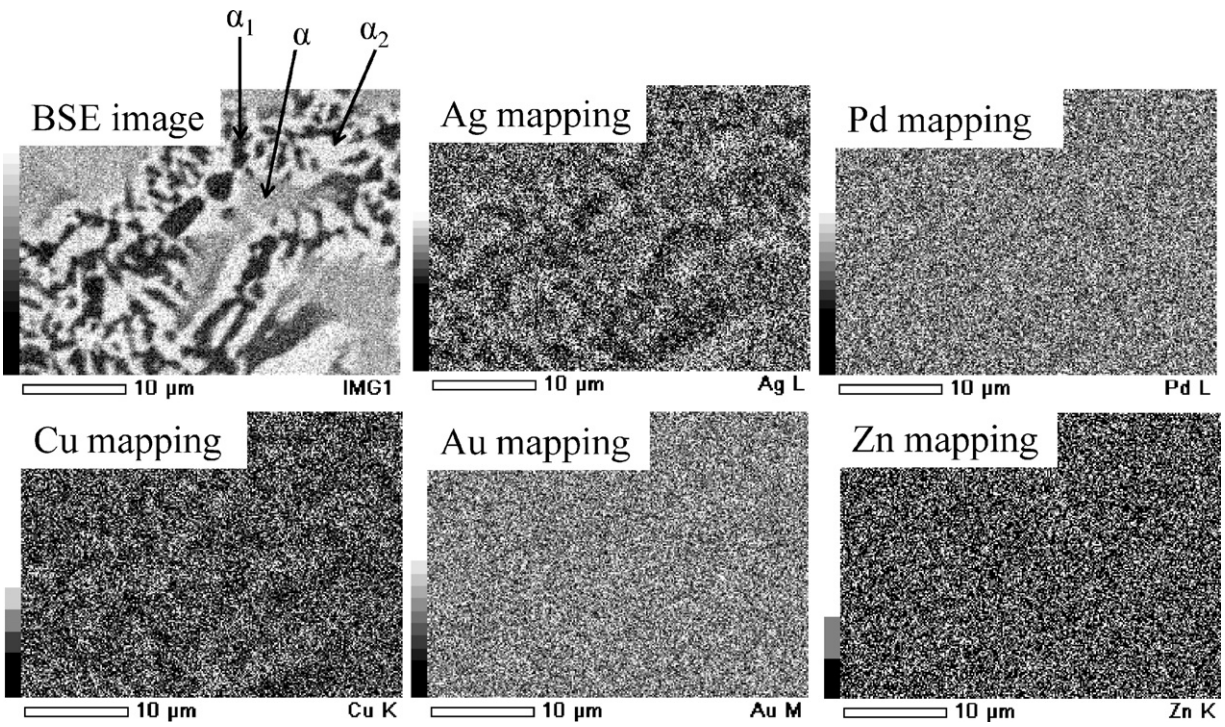

Fig. 12. BSE image and results of EDX analysis on specimen surface of 1023WQ$_{LRS}$/28.8 ks.

β phase precipitated in 673WQ$_{LRS}$/1.8 ks is dissolved by ST at 1173 K.

3.2. Hardness

3.2.1. Effect of solution treatment on hardness of CR

Fig. 18 shows the change in Vickers hardness of CR and CR-ST. The hardness of CR-ST, where the fine $L1_0$-type ordered β′ phase is densely precipitated, increases drastically. This result well agrees with the previous studies [4,5], which found that the precipitation of the β′ phase in the matrix contributes to the unique hardening behavior of CR-ST.

3.2.2. Effect of solution treatment on hardness of LRS

Fig. 19 shows the change in Vickers hardness of 1173WQ$_{LRS}$/3.6 ks and 1023WQ$_{LRS}$/1.8–28.8 ks. The change in

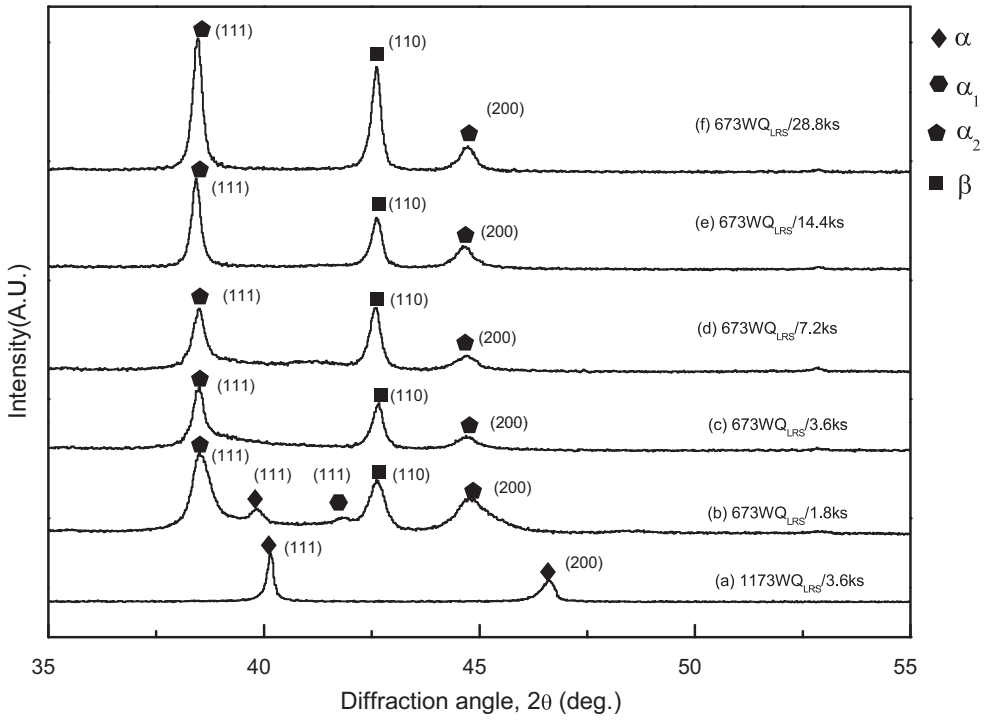

Fig. 13. XRD profiles of (a) 1173WQ$_{LRS}$/3.6 ks, (b) 1023WQ$_{LRS}$/1.8 ks, (c) 1023WQ$_{LRS}$/3.6 ks, (d) 1023WQ$_{LRS}$/7.2 ks, (e) 1023WQ$_{LRS}$/14.4 ks and (f) 1023WQ$_{LRS}$/28.8 ks.

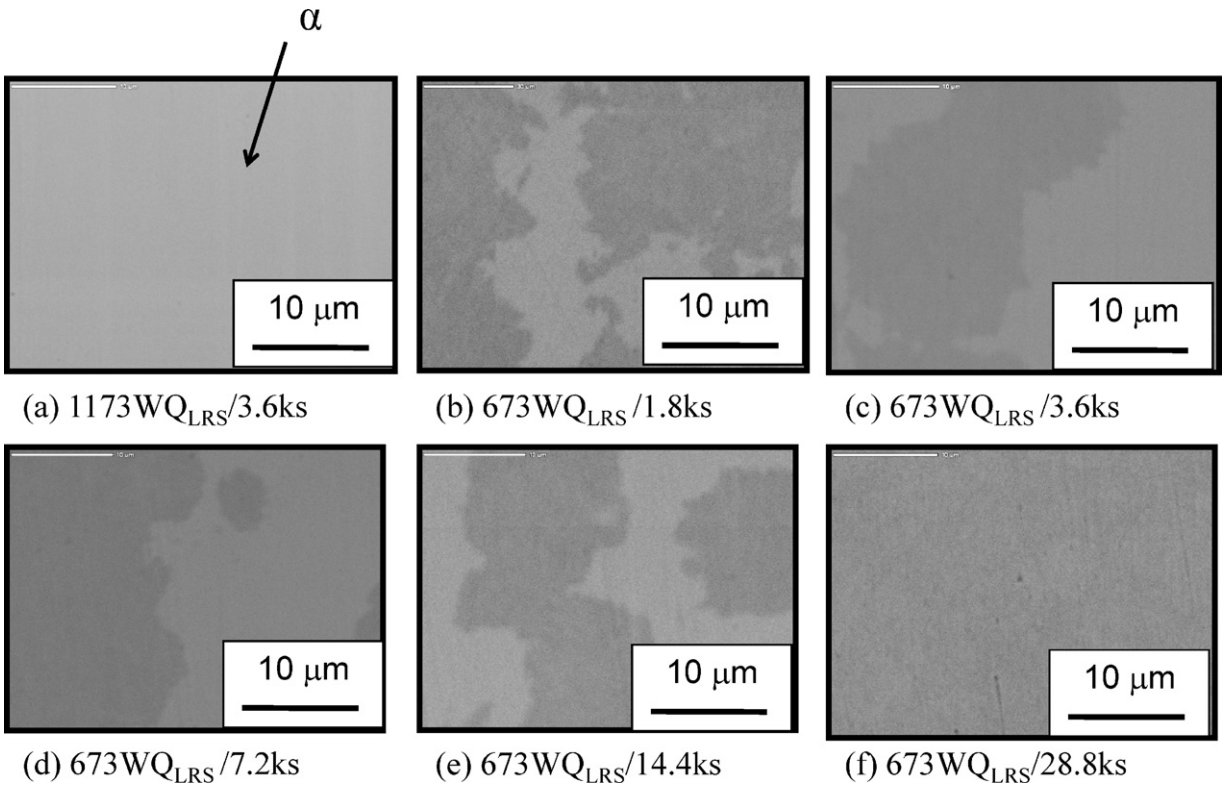

Fig. 14. BSE images of (a) 1173WQ$_{LRS}$/3.6 ks, (b) 673WQ$_{LRS}$/1.8 ks, (c) 673WQ$_{LRS}$/3.6 ks, (d) 673WQ$_{LRS}$/7.2 ks, (e) 673WQ$_{LRS}$/14.4 ks and (f) 673WQ$_{LRS}$/28.8 ks.

hardness is small among them even though the α_1 and α_2 phases are decomposed from 1173WQ$_{LRS}$/3.6 ks with the single α phase by ST at 1023 K. Therefore, it seems that the effect of decomposition of α_1 and α_2 phases on the unique hardening behavior is small.

3.2.3. Effect of aging treatment on hardness of LRS

Fig. 20 shows Vickers hardness in 1173WQ$_{LRS}$/3.6 ks and 673WQ$_{LRS}$/1.8–28.8 ks. The hardness of 673WQ$_{LRS}$/1.8 ks with the precipitated β phase increases greatly compared with that of 1173WQ$_{LRS}$/3.6 ks with the single α phase. The hardness of

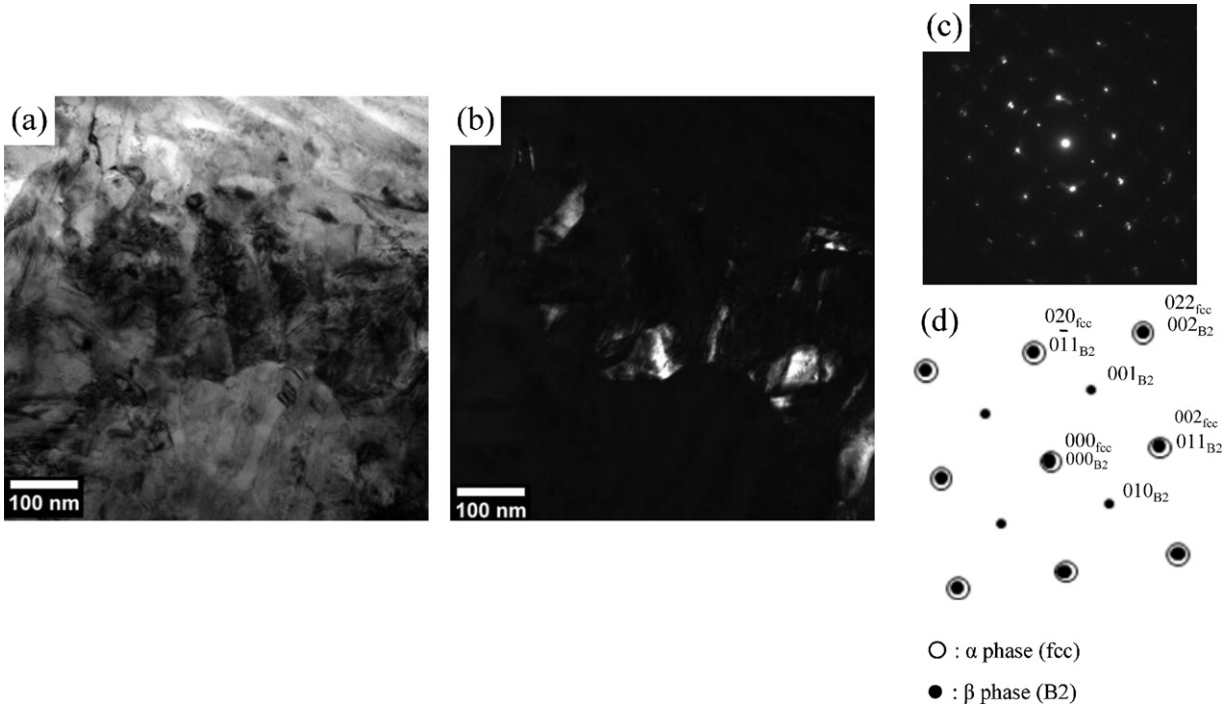

Fig. 15. Results of TEM observation of 673WQ$_{LRS}$/1.8 ks: (a) bright field image, (b) dark field image by using a 0 1 0 superlattice reflection, (c) selected area diffraction pattern and (d) key diagram. Beam direction is parallel to [1 0 0].

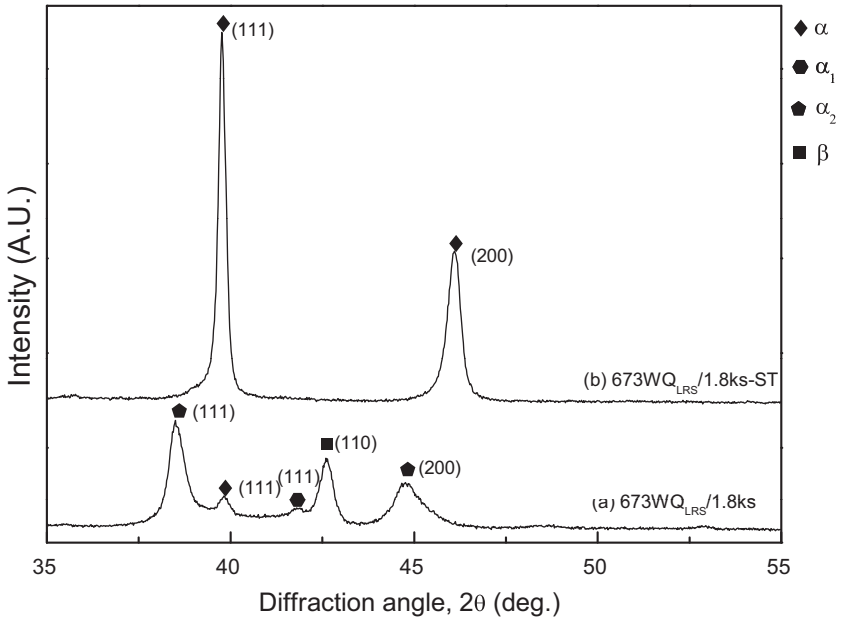

Fig. 16. XRD profiles of 673WQ$_{LRS}$/1.8 ks, 673WQ$_{LRS}$/1.8 ks-ST.

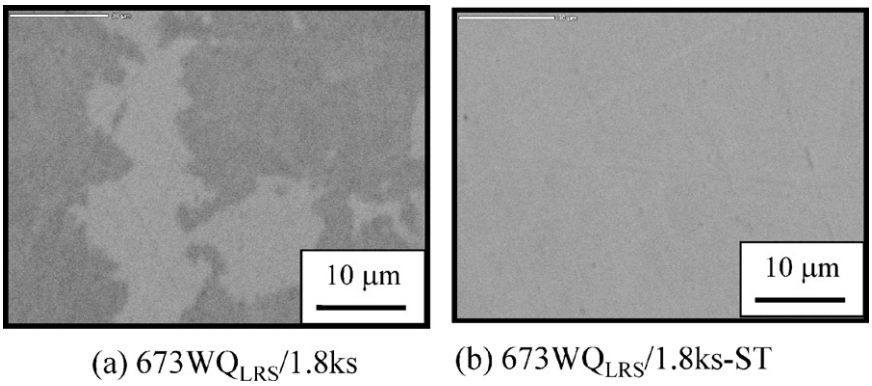

Fig. 17. BSE images of (a) 673WQ$_{LRS}$/1.8 ks and (b) 673WQ$_{LRS}$/1.8 ks-ST.

673WQ$_{LRS}$/7.2 ks is the highest and then the hardness tends to decrease.

Fig. 21 shows the change of Vickers hardness on 673WQ$_{LRS}$/1.8 ks and 673WQ$_{LRS}$/1.8 ks-ST. The hardness of 673WQ$_{LRS}$/1.8 ks decreases with the dissolution of the β phase by ST.

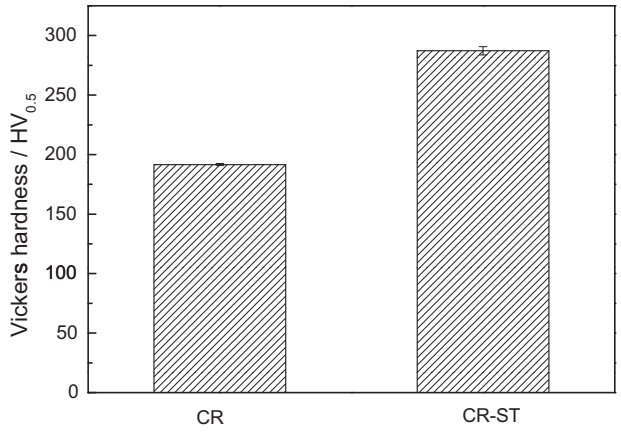

Fig. 18. Vickers hardness of CR and CR-ST.

According to these results, the L1$_0$-type ordered β′ phase precipitated in the matrix by ST may strongly contribute to the hardening in the case of Ag–20Pd–14.5Cu–12Au alloy fabricated by cold rolling. However, the β phase precipitated in the matrix by AT may strongly contribute to the hardening in the case of Ag–20Pd–14.5Cu–12Au alloy fabricated by LRS.

4. Discussion

The decomposition of α_1 and α_2 phases weakly contributes to the hardening in Ag–20Pd–14.5Cu–12Au alloy. The precipitation of the β′ or β phase in the matrix seems to contribute to the hardening strongly in Ag–20Pd–14.5Cu–12Au alloy. In the case of CR, the hardness increases drastically by ST. The diameter of β phase remaining after ST is several μm (Fig. 8) and the size of lath-shaped β′ phase precipitated after ST is several nm width and about 100 nm length (Fig. 9). In the case of LRS, the hardness increases by AT. While the β′ phase is not precipitated by AT, the diameter of β phase precipitated by AT in the 673WQ$_{LRS}$/1.8 ks is several 10 nm length (Fig. 15). The crystal structure of β phase remained in the CR-ST and the β phase precipitated in the 673WQ$_{LRS}$/1.8 ks are identified as being

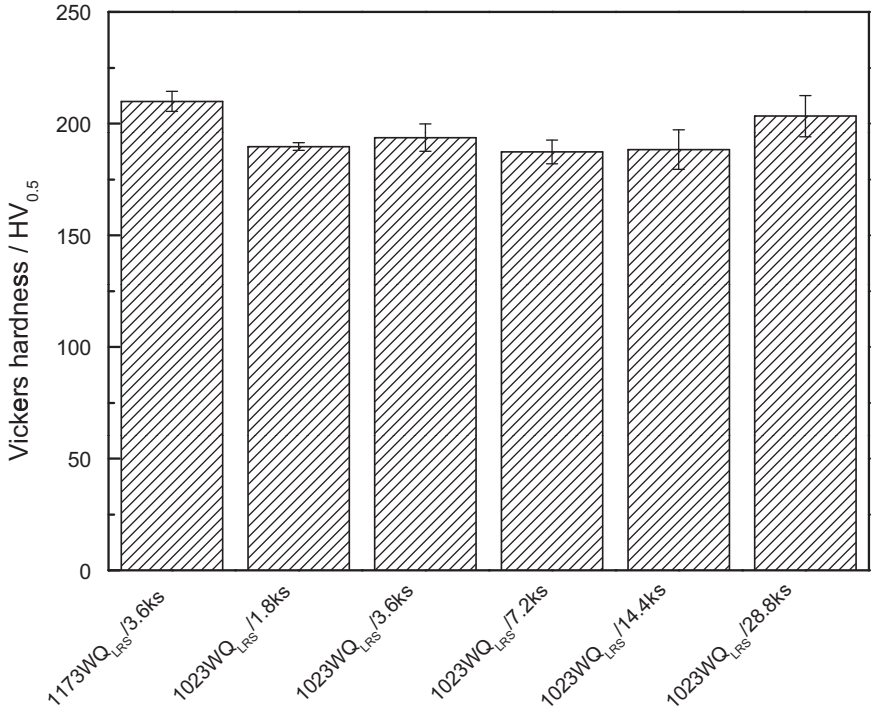

Fig. 19. Vickers hardness of $1173WQ_{LRS}$/3.6 ks, $1023WQ_{LRS}$/1.8 ks, $1023WQ_{LRS}$/3.6 ks, $1023WQ_{LRS}$/7.2 ks, $1023WQ_{LRS}$/14.4 ks and $1023WQ_{LRS}$/28.8 ks.

the same B2-type ordered structure by XRD analysis. However, it has been found that their size and shape are different. Furthermore, it was found by XRD profiles that the fine β phase precipitated in $673WQ_{LRS}$/1.8 ks is dissolved by ST while the β phase existed in CR is not dissolved by ST. Generally, the phase that strongly contributes to the hardening is the fine precipitates, which cause strain in the matrix. In CR-ST, there are two precipitates (β′, β). It is supposed that the precipitation of β phase may contribute to the hardness increase of CR-ST from the result of $673WQ_{LRS}$/1.8 ks. However, the β phase remaining in CR-ST is coarse. The β′ phase in CR-ST is fine and is densely precipitated. Therefore, it could be concluded that effect of the precipitation of the fine β′ phase on the hardening behavior is strong. Although the macro chemical compositions of CR and LRS are the same, the micro chemical composition of the matrix (α phase) is thought to be different due to the existence of the coarse Cu–Pd β phase, which is not dissolved by ST. That is, the matrix (α phase) of CR with the coarse Cu–Pd β phase, which is not dissolved by ST, has a higher Ag concentration than the matrix (α

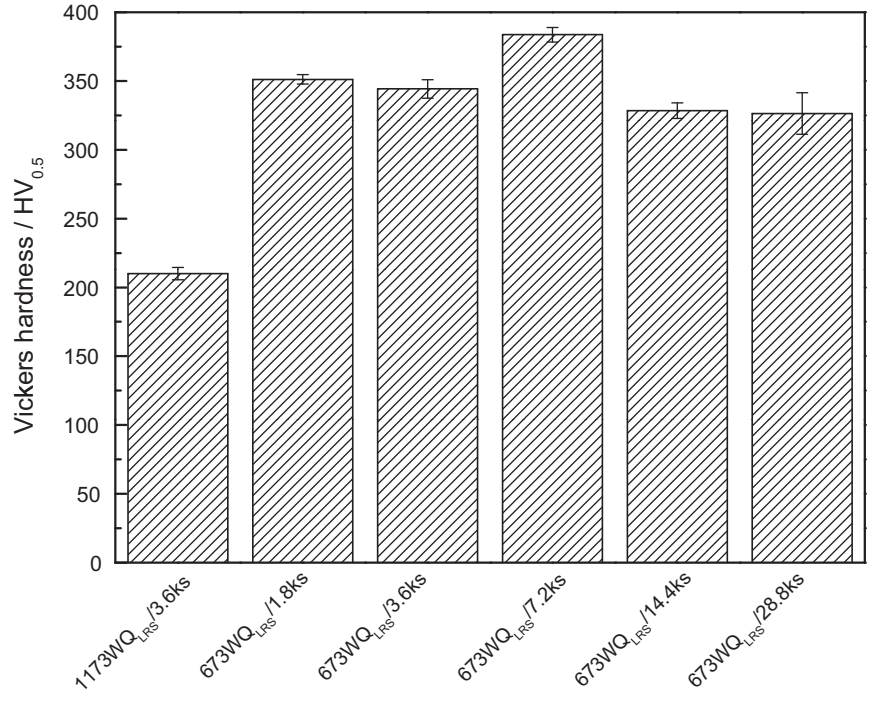

Fig. 20. Vickers hardness of $1173WQ_{LRS}$/3.6 ks, $673WQ_{LRS}$/1.8 ks, $673WQ_{LRS}$/3.6 ks, $673WQ_{LRS}$/7.2 ks, $673WQ_{LRS}$/14.4 ks and $673WQ_{LRS}$/28.8 ks.

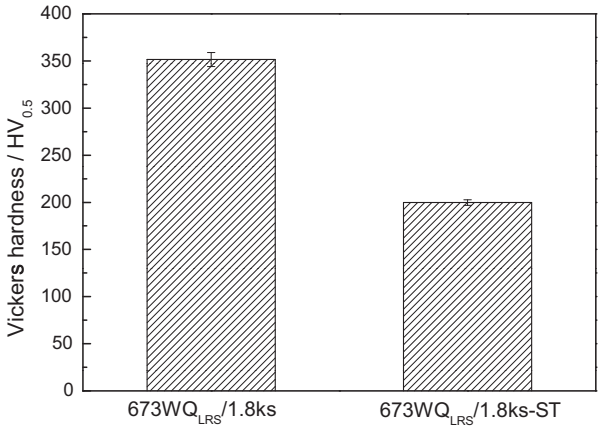

Fig. 21. Vickers hardness of 673WQ_{LRS}/1.8 ks and 673WQ_{LRS}/1.8 ks-ST.

phase) of LRS. It is considered that the β′ phase is precipitated in the Ag-rich matrix, which has a high Ag concentration due to the existence of a coarse Cu–Pd β phase.

5. Conclusions

The microstructural change and hardness change in Ag–20Pd–12Au–14.5Cu alloy fabricated by cold rolling and Ag–20Pd–12Au–14.5Cu alloy fabricated by the liquid rapid solidification method through various heat treatments were examined to investigate the effect of constitutional phases on the unique hardening behaviors of as-solutionized Ag–20Pd–12Au–14.5Cu alloy. The obtained results are as follows:

(1) The hardness of Ag–20Pd–12Au–14.5Cu alloy fabricated by cold rolling increases and the fine $L1_0$-type ordered β′ phase is precipitated densely while the coarse B2-type ordered β phase is remained in the matrix after solution treatment. These findings agree with those of previous studies.

(2) The single α phase of Ag–20Pd–14.5Cu–12Au alloy fabricated by LRS method decomposes into α_1 and α_2 by solution treatment at 1023 K and the hardness changes slightly.

(3) The single α phase of Ag–20Pd–14.5Cu–12Au alloy fabricated by LRS changes into α_1 and α_2 phase and the β phase is precipitated by aging treatment at 673 K, and the hardness increases greatly. The precipitated β phase is dissolved and the hardness decreases by solution treatment at 1173 K for 3.6 ks.

Therefore, it is considered that the precipitation of fine $L1_0$-type ordered β′ phase contributes strongly to the unique hardening behavior in as-solutionized dental Ag–20Pd–12Au–14.5Cu alloy while the coarse B2-type ordered β phase remaining after solution treatment and the decomposition of Cu rich phase and Ag rich phase contribute weakly to the hardness increase.

Acknowledgements

The authors would like to thank the support of Ishifuku Metal Industry Co., Ltd. for this research. This study was financially supported in part by the Grant-in-aid for Scientific Research from Japan Society for the Promotion of Science (#21360332) and the Global COE program “Materials Integration International Center of Education and Research, Tohoku University”, Ministry of Education, Culture, Sports, Science and Technology (MEXT) of Japan.

References

[1] M. Ohta, T. Shiraish, K. Hisatsune, M. Yamane, Age-hardening of dental Ag–Pd–Cu–Au alloys, J. Dent. Res. 59 (1980) 1966–1971.
[2] C.H. Yu, M.G. Park, Y.H. Kwon, H.J. Seol, H.I. Kim, Phase transformation and microstructural changes during ageing process of an Ag–Pd–Cu–Au alloy, J. Alloys Compd. 460 (2008) 331–336.
[3] H. Fukui, S. Shinoda, M. Mukai, K. Yasue, J. Hasegawa, Effect of heat treatment on mechanical properties of type IV gold and 12 wt.% Au–Pd–Ag alloys, J. Jpn. Dent. Mater. 11 (1992) 141–148.
[4] Y. Tanaka, H.J. Seol, T. Ogata, E. Miura, T. Shiraishi, K. Hisatsune, Hardening mechanism of dental casting gold–silver–palladium alloy by higher-temperature heat-treatment, J. Jpn. Dent. Mater. 22 (2003) 69.
[5] T. Akahori, M. Niinomi, M. Nakai, H. Tsutsumi, T. Kanno, Y.H. Kim, H. Fukui, Relationship between unique hardening behavior and microstructure of dental silver alloy subjected to solution treatment, J. Jpn. Inst. Met. 74 (2010) 337–344.